*J. Fluid Mech.* (2008), *vol.* 614, *pp.* 407–424. © 2008 Cambridge University Press 
doi:10.1017/S0022112008003303 Printed in the United Kingdom

# Discontinuous solutions of the boundary-layer equations

A. I. RUBAN AND K. N. VONATSOS
Department of Mathematics, University of Manchester, Oxford Road, Manchester M13 9PL, UK

(Received 5 December 2007 and in revised form 7 July 2008)

Since 1904, when Prandtl formulated the boundary-layer equations, it has been presumed that due to the viscous nature of the boundary layers the solution of the Prandtl equations should be sought in the class of continuous functions. However, there are clear mathematical reasons for discontinuous solutions to exist. Moreover, under certain conditions they represent the only possible solutions of the boundary-layer equations.

In this paper we consider, as an example, an unsteady analogue of the laminar jet problem first studied by Schlichting in 1933. In Schlichting's formulation the jet emerges from a narrow slit in a flat barrier and penetrates into a semi-infinite region filled with fluid which would remain at rest if the slit were closed. Assuming the flow steady, Schlichting was able to demonstrate that the corresponding solution to the Prandtl equations may be written in an explicit analytic form. Here our concern will be with unsteady flow that is initiated when the slit is opened and the jet starts penetrating into the stagnant fluid. To study this process we begin with the numerical solution of the unsteady boundary-layer equations. Since discontinuities were expected, the equations were written in conservative form before finite differencing. The solution shows that the jet has a well-established front representing a discontinuity in the velocity field, similar to the shock waves that form in supersonic gas flows.

Then, in order to reveal the 'internal structure' of the shock we turn to the analysis of the flow in a small region surrounding the discontinuity. With $Re$ denoting the Reynolds number, the size of the inner region is estimated as an order $Re^{-1/2}$ quantity in both longitudinal and lateral directions. We found that the fluid motion in this region is predominantly inviscid and may be treated as quasi-steady if considered in the coordinate frame moving with the jet front. These simplifications allow a simple formula for the front speed to be deduced, which proved to be in close agreement with experimental observation of Turner (*J. Fluid Mech.* vol. 13 (1962), p. 356).

## 1. Introduction

More than a hundred years have passed since the 3rd International Mathematics Congress in Heidelberg, where Prandtl presented his seminal paper (see Prandtl 1904) on the boundary-layer theory. In this paper, Prandtl put forward an important idea which later became the foundation of the theory of singular perturbations. On the basis of this idea Prandtl deduced the boundary-layer equations governing the fluid motion near a rigid body surface at large values of the Reynolds number, $Re$. At that time Prandtl did not offer any solutions to the boundary-layer equations. Instead, he speculated at length on the separation phenomenon. According to Prandtl, the separation can be expected when the pressure rises along the body surface, causing

https://doi.org/10.1017/S0022112008003303 Published online by Cambridge University Press

the flow in the boundary layer to decelerate. He argued that the separation takes place at the point of zero skin friction, the position of which could be determined through solving the boundary-layer equations.

Later, however, it became clear that the boundary-layer theory in its classical form, as formulated by Prandtl (1904), leads to a mathematical contradiction associated with Goldstein's (1948) singularity. A key element of the separation process, which was not fully appreciated in Prandtl's description, was an interaction between the boundary layer and external inviscid flow, now referred to as the *viscous–inviscid interaction*. Asymptotic theory of the viscous–inviscid interaction, also known as the *triple-deck theory*, was formulated simultaneously by Neiland (1969) and Stewartson & Williams (1969) for the self-induced separation in supersonic flow and by Stewartson (1969) and Messiter (1970) for incompressible fluid flow near the trailing edge of a flat plate. Applying this theory to the original Prandtl's problem of the incompressible flow separation from a blunt body surface, Sychev (1972) demonstrated that the boundary-layer separation takes place not as a result of a gradual growth of pressure along the body surface; instead, it is caused by a sharp pressure rise developing 'spontaneously' due to the viscous–inviscid interaction at a location on the body surface where, according to Prandtl's theory, the boundary layer would still be well attached.

Later many researchers were involved in the development of the theory, and it became clear that the viscous–inviscid interaction plays a key role in a wide variety of fluid dynamic phenomena. An exposition of applications of the theory to different forms of the boundary-layer separation may be found, for example, in the monograph by Sychev *et al.* (1998).

Summarizing the results of a century long effort in this field, one can see, however, that despite the significance of the progress made, many aspects of the theory of separated flows remain unresolved. Most notably, the theory remains predominantly restricted to situations when the separating flow may be treated as two-dimensional and steady. Much less is know about three-dimensional and/or unsteady separation. The reason for this is not just that an additional independent variable increases the difficulty in constructing solutions of the governing equations. More importantly, for three-dimensional and unsteady flows alternative forms of separation become possible, which might not even involve the flow reversal.

In particular, it is known (see Stewartson, Cebeci & Chang 1980; Kluwick & Wohlfahrt 1986; Allen & Riley 1994) that three-dimensional boundary layers often develop the so-called *collisional singularity*. It is observed in situations where the fluid particles converge in their lateral motion in the boundary layer near the body surface, resulting in displacement of streamlines from the wall and possible eruption of the fluid from the boundary layer. Similar processes are also observed in two-dimensional unsteady boundary layers. A well-known example is the boundary-layer separation at the leading edge of a pitching up aerofoil. It was studied by various authors. In particular, Degani, Li & Walker (1996) produced a numerical solution for the unsteady boundary-layer equations assuming that the angle of attack $\alpha$ increases with time to a maximum value $\alpha_{\max}$. They found that if $\alpha_{\max}$ exceeds a certain critical value $\alpha^*$, which is dependent on the aerofoil shape, then a singularity develops in the boundary layer at a finite time $t_0$. It leads to activation (in a small vicinity of the singular point) of the viscous–inviscid interaction process, when the displacement effect of the boundary layer can no longer be disregarded, and should be taken into account to calculate the pressure gradient in the inviscid part of the flow. However, this flow regime is short-lived, and a more important question is: what happens 'on

https://doi.org/10.1017/S0022112008003303 Published online by Cambridge University Press

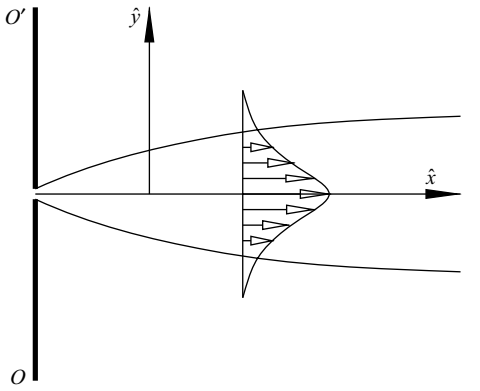



FIGURE 1. Problem layout.

the other side of the singularity', i.e. when $t > t_0$. We believe that the analysis of the 'post-catastrophic' behaviour of the flow may be conducted based on discontinuous solutions of the boundary-layer equations. The main objective of this paper is to demonstrate the existence of such solutions. To perform this task we will consider, as an example, the unsteady analogue of the laminar jet studied first by Schlichting (1933).

In Schlichting's formulation it was assumed that the jet emerges from a narrow slit in a flat barrier $OO'$, as shown in figure 1, and mixes with the surrounding fluid on the right-hand side of the barrier. The governing boundary-layer equations have the form

$$\hat{u}\frac{\partial \hat{u}}{\partial \hat{x}} + \hat{v}\frac{\partial \hat{u}}{\partial \hat{y}} = \nu\frac{\partial^2 \hat{u}}{\partial \hat{y}^2}, \tag{1.1a}$$

$$\frac{\partial \hat{u}}{\partial \hat{x}} + \frac{\partial \hat{v}}{\partial \hat{y}} = 0. \tag{1.1b}$$

Here $(\hat{x}, \hat{y})$ are Cartesian coordinates, $\hat{x}$ is measured along the axis of the jet from the slit and $\hat{y}$ in the perpendicular direction; the velocity components in these coordinates are $\hat{u}$ and $\hat{v}$, respectively; $\nu$ is the kinematic viscosity coefficient. The 'hat' is used here to show that the corresponding variables are dimensional.

Equations (1.1) should be solved with the symmetry conditions on the jet axis

$$\hat{v} = \frac{\partial \hat{u}}{\partial \hat{y}} = 0 \quad \text{at} \quad \hat{y} = 0, \tag{1.2}$$

and the condition of matching with the stagnant fluid surrounding the jet

$$\hat{u} \to 0 \quad \text{as} \quad \hat{y} \to \infty. \tag{1.3}$$

Schlichting (1933) found that the boundary-value problem (1.1)–(1.3) admits a self-similar solution which is written in terms of the stream function $\hat{\psi}$ as

$$\hat{\psi} = \nu\hat{x}^{1/3} f(\eta), \qquad \eta = \frac{\hat{y}}{\hat{x}^{2/3}}. \tag{1.4}$$

Recall that the stream function is related to the velocity components via the equations

$$\hat{u} = \frac{\partial \hat{\psi}}{\partial \hat{y}}, \qquad \hat{v} = -\frac{\partial \hat{\psi}}{\partial \hat{x}}.$$

https://doi.org/10.1017/S0022112008003303 Published online by Cambridge University Press

Solution (1.4) can be used to describe the flow in the jet provided that the slit width is small as compared to the thickness of the jet.

Interestingly, function $f(\eta)$ in (1.4) may be expressed in a simple analytical form,

$$f(\eta) = 3C\frac{1-\exp(-C\eta)}{1+\exp(-C\eta)}, \tag{1.5}$$

with constant $C$ being a function of the fluid momentum flux $M$ through the slit. The latter remains constant in the jet. Indeed, multiplying the continuity equation (1.1$b$) by $\hat{u}$ and adding the result to the momentum equation (1.1$a$) results in

$$\frac{\partial}{\partial\hat{x}}(\hat{u}^2)+\frac{\partial}{\partial\hat{y}}(\hat{u}\hat{v})=\nu\frac{\partial^2\hat{u}}{\partial\hat{y}^2},$$

which, being integrated across the jet shows that the momentum flux

$$M=\rho\int_{-\infty}^{\infty}\hat{u}^2\,\mathrm{d}\hat{y} \tag{1.6}$$

is independent of $\hat{x}$.

In this paper we consider an unsteady analogue of the Schlichting problem. We assume that at the beginning the slit (see figure 1) was closed, and the fluid to the right of the barrier $OO'$ was stagnant. Then, at time $\hat{t}=0$ the slit opens, and the jet starts penetrating into the stagnant fluid. To describe this process we shall start by solving the unsteady boundary-layer equations. They are valid if the characteristic Reynolds number, $Re$, is large. Since discontinuities are expected in the solution, the boundary-layer equations are written in a conservative form (§2) before finite differencing. The results of the calculations are presented in §3. In particular, we found that the jet has a well-established front which propagates away from the jet source with a finite speed. Everywhere before this front the fluid remains at rest; behind the front it moves with a finite velocity. This creates a discontinuity in the velocity field, similar to the shock waves in gas dynamics.

We shall call the discontinuities in boundary-layer flows *pseudo-shocks*. The reason for the name may be explained as follows. It is known that the characteristic thickness of the classical shock waves in gas dynamics is comparable with the molecular mean free path, which makes continuum approach inapplicable for describing their internal structure. Instead the Boltzmann equation of the kinetic gas theory should be used. As far as the jet flow is concerned, we shall demonstrate in §4 that the velocity jump observed at the jet front is 'smoothed out' over a much larger distance, $O(Re^{-1/2})$, and therefore, the internal structure of the pseudo-shock may be studied using the Navier–Stokes equation. It appears that at large values of the Reynolds number, $Re$, the fluid motion in the $O(Re^{-1/2})$ region near the jet front is predominantly inviscid and may be treated as quasi-steady if considered in the coordinate frame moving with the jet front. An important outcome of our analysis is that the velocity of the shock is precisely half the maximum velocity of the fluid in the jet immediately behind the pseudo-shock. This proved to be in close agreement with experimental observation of Turner (1962).

We also found that the main physical process that takes place in the inner $O(Re^{-1/2})$ region is the 'collision' of the jet with the uniform flow approaching (in the moving coordinates) from the opposite direction. As a result of the collision the fluid is forced to erupt from the jet. This process was earlier discussed by Stewartson *et al.* (1980) and Kluwick & Wohlfahrt (1986) in connection with the so-called 'collisional separation' of three-dimensional steady boundary layers.

https://doi.org/10.1017/S0022112008003303 Published online by Cambridge University Press

## 2. Formulation of the problem

Let $(\hat{x}, \hat{y})$ be again Cartesian coordinates; $\hat{x}$ is measured from the centre of the slit in the direction normal to the barrier $OO'$, and $\hat{y}$ parallel to $OO'$ (see figure 1). The velocity components in these coordinates are denoted as $\hat{u}$ and $\hat{v}$, respectively. Further let $\hat{t}$ be time and $\hat{p}$ pressure. In what follows we restrict our attention to incompressible fluid with constant density $\rho$ and constant kinematic viscosity coefficient $\nu$.

In order to write the governing equations in dimensionless form we choose an observation position at some distance $L$ from the slit, and denote the characteristic fluid velocity in the jet by $U_0$; the latter being dependent on the fluid momentum flux through the slip. With $P_0$ denoting the pressure in the stagnant fluid surrounding the jet, the non-dimensional variables may be introduced through the scalings

$$\left.\begin{aligned} \hat{u} &= U_0 u, \qquad \hat{v} = U_0 Re^{-1/2} V, \qquad \hat{p} = P_0 + \rho U_0^2 p, \\ \hat{x} &= Lx, \qquad \hat{y} = LRe^{-1/2} Y, \qquad \hat{t} = \tfrac{L}{U_0} t. \end{aligned}\right\} \tag{2.1}$$

Here

$$Re = \frac{U_0 L}{\nu}$$

is the Reynolds number. If $Re$ is large, then the boundary-layer equations

$$\frac{\partial u}{\partial t} + u\frac{\partial u}{\partial x} + V\frac{\partial u}{\partial Y} = -\frac{\partial p}{\partial x} + \frac{\partial^2 u}{\partial Y^2}, \tag{2.2a}$$

$$\frac{\partial p}{\partial Y} = 0, \tag{2.2b}$$

$$\frac{\partial u}{\partial x} + \frac{\partial V}{\partial Y} = 0. \tag{2.2c}$$

may be used to study the behaviour of the jet.

We shall assume (subject to subsequent confirmation) that in the fluid surrounding the jet, the pressure remains unchanged $\hat{p} = P_0$ in the leading-order approximation. Then, using (2.2*b*), we can conclude that the non-dimensional pressure $p$ appears to be zero also inside the jet, in which case (2.2) reduce to

$$\frac{\partial u}{\partial t} + u\frac{\partial u}{\partial x} + V\frac{\partial u}{\partial Y} = \frac{\partial^2 u}{\partial Y^2}, \tag{2.3a}$$

$$\frac{\partial u}{\partial x} + \frac{\partial V}{\partial Y} = 0. \tag{2.3b}$$

Similar to its steady counterpart (1.1*a*), the momentum equation (2.3*a*) is, of course, parabolic, but now it acquires a hyperbolic sub-operator

$$\frac{\partial u}{\partial t} + u\frac{\partial u}{\partial x},$$

with the trajectories of the fluid particles playing the role of the characteristics in the $(t, x)$-plane. When they converge, the solution develops a *collisional singularity*, leading to a discontinuity in the velocity field. In order to study such discontinuities,

https://doi.org/10.1017/S0022112008003303 Published online by Cambridge University Press

conservative form of the boundary-layer equations (2.3) should be used,

$$\frac{\partial u}{\partial t} + \frac{\partial (u^2)}{\partial x} + \frac{\partial}{\partial Y}\left(uV - \frac{\partial u}{\partial Y}\right) = 0, \tag{2.4a}$$

$$\frac{\partial u}{\partial x} + \frac{\partial V}{\partial Y} = 0. \tag{2.4b}$$

Equations (2.4*a*) and (2.4*b*) have to be solved with the symmetry conditions on the jet axis

$$V = \frac{\partial u}{\partial Y} = 0 \quad \text{at} \quad Y = 0, \quad x \in (0, \infty), \tag{2.4c}$$

and the condition of matching with the stagnant fluid around the jet

$$u \to 0 \quad \text{as} \quad Y \to \infty, \quad x \in (0, \infty). \tag{2.4d}$$

We also need to know the distribution of the longitudinal velocity across the slit. We shall assume, to make it simple, that

$$u\Big|_{x=0} = \begin{cases} 1 - Y^2 & \text{if} \quad |Y| \leqslant 1, \\ 0 & \text{if} \quad |Y| > 1. \end{cases} \tag{2.4e}$$

Finally, the initial conditions can be written as

$$u = V = 0 \quad \text{at} \quad t = 0, \quad x \in [0, \infty), \quad Y \in (-\infty, \infty). \tag{2.4f}$$

## 3. Numerical results

For numerical solution of the initial value problem in (2.4) an implicit Euler scheme was used. In this scheme the solution is constructed by progressing in time. At each time step, the velocity field in the $(x, Y)$-domain is found by marching in the $x$-direction; at each $x$-position iterations are used to find the distributions of the two velocity components in the $Y$-direction. During each iteration the momentum equation (2.4*a*) is solved first to update the distribution of $u$. Then $V$ is updated using the continuity equation (2.4*b*). This procedure is repeated until a pre-defined tolerance is achieved. Then we move to the next $x$-station.

Since discontinuities were expected in the solution, low-order approximations were used when discretizing equations (2.4*a*) and (2.4*b*). A uniform grid

$$\{x_i, Y_j, t_k\}$$

was employed in this study. The momentum equation (2.4*a*) was finite-differenced on the basis of the stencil shown in figure 2. The resulting algebraic equations were linearized as follows. For the first nonlinear term $u^2$ in (2.4*a*) the Newton–Raphson procedure was used, namely, at each point $(x_i, Y_j, t_k)$ we wrote

$$u^2 = 2\bar{u}u - \bar{u}^2.$$

Here, $\bar{u}$ denotes the value of the longitudinal velocity component at the previous iteration. The second nonlinear term $uV$ was linearized by simply taking $V$ from the previous iteration, i.e. $uV = u\bar{V}$. The quantities at the middle points of the stencil (see figure 2) were evaluated using the simple averaging formula,

$$V^k_{i,j\pm\frac{1}{2}} = \tfrac{1}{2}\left(V^k_{i,j\pm1} + V^k_{i,j}\right).$$

https://doi.org/10.1017/S0022112008003303 Published online by Cambridge University Press

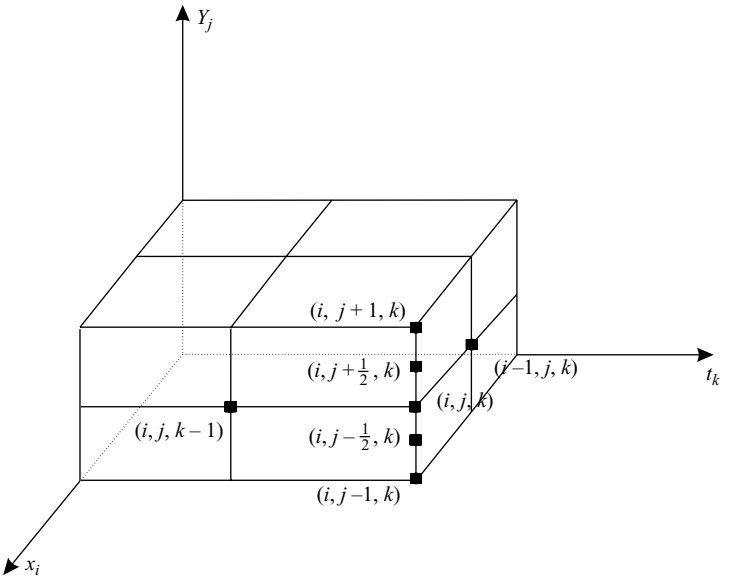



FIGURE 2. The stencil used for finite-differencing equation (2.4*a*).

This approach leads to the following representation of the terms in equation (2.4*a*),

$$\frac{\partial u}{\partial t} = \frac{u^k_{i,j} - u^{k-1}_{i,j}}{\Delta t},$$

$$\frac{\partial (u^2)}{\partial x} = \frac{\left(u^k_{i,j}\right)^2 - \left(u^k_{i-1,j}\right)^2}{\Delta x} = \frac{2\bar{u}^k_{i,j}}{\Delta x} u^k_{i,j} - \frac{\left(\bar{u}^k_{i,j}\right)^2 + \left(u^k_{i-1,j}\right)^2}{\Delta x},$$

$$\frac{\partial (uV)}{\partial Y} = \frac{u^k_{i,j+\frac{1}{2}} V^k_{i,j+\frac{1}{2}} - u^k_{i,j-\frac{1}{2}} V^k_{i,j-\frac{1}{2}}}{\Delta Y}$$

$$= \frac{\bar{V}^k_{i,j+1} + \bar{V}^k_{i,j}}{4\Delta Y} u^k_{i,j+1} + \frac{\bar{V}^k_{i,j+1} - \bar{V}^k_{i,j-1}}{4\Delta Y} u^k_{i,j} - \frac{\bar{V}^k_{i,j} + \bar{V}^k_{i,j-1}}{4\Delta Y} u^k_{i,j-1},$$

$$\frac{\partial^2 u}{\partial Y^2} = \frac{1}{\Delta Y^2} u^k_{i,j+1} - \frac{2}{\Delta Y^2} u^k_{i,j} + \frac{1}{\Delta Y^2} u^k_{i,j-1}.$$

This leads to a tridiagonal set of equations for $u^k_{i,j}$, $j = 0, \ldots, J$, which was solved using the Thomas technique. Then the lateral velocity component $V$ was updated (at given time $t_k$ and the mesh line considered $x_i$) through recursive use of the formula

$$V^k_{i,j} = \frac{u^k_{i-1,j} - u^k_{i,j}}{\Delta x} \Delta Y + V^k_{i,j-1}, \qquad j = 1, \ldots, J, \tag{3.1}$$

which is obtained by finite differencing of the continuity equation (2.4*b*). To start the calculations in (3.1), the symmetry condition, $V^k_{i,1} = 0$, was used.

The results of the calculations are presented in figure 3, where the distribution of the fluid velocity along the jet axis is shown at different times. We see that the solution develops a discontinuity (pseudo-shock) which propagates in the positive $x$-direction as time $t$ increases. In front of the shock the fluid remains at rest. Immediately behind the shock it has a finite velocity. Surprisingly enough, at $Y = 0$ the distribution of the velocity behind the shock follows very closely the steady solutions (1.4) and (1.5). For comparison, we show in figure 4 the behaviour of the longitudinal velocity $u$ at

https://doi.org/10.1017/S0022112008003303 Published online by Cambridge University Press

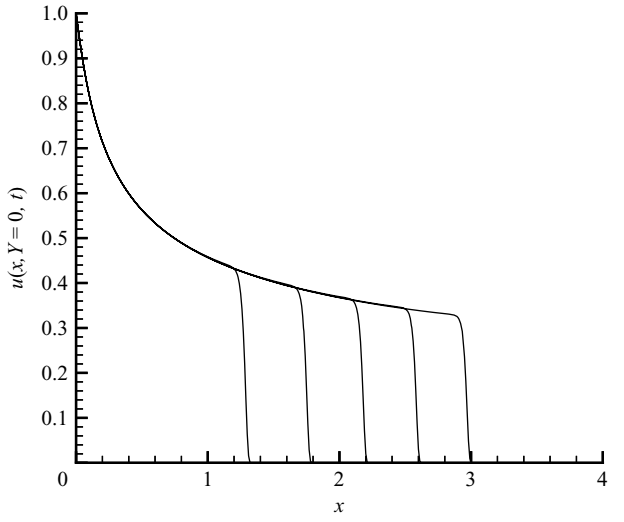



FIGURE 3. Velocity distribution along the jet axis at $t = 4$, 6, 8, 10 and 12.

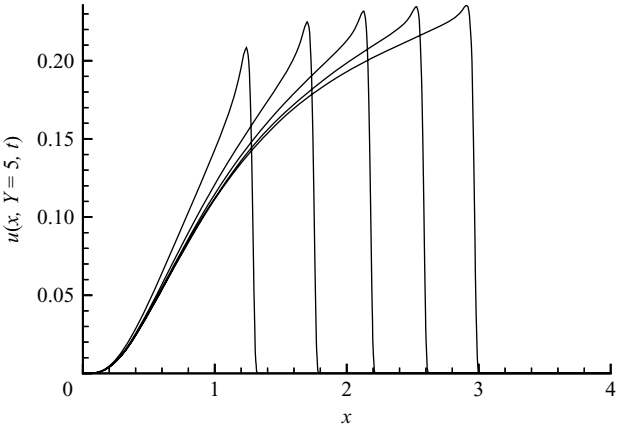



FIGURE 4. Longitudinal velocity distribution at level $Y = 5$ above the jet axis at $t = 4$, 6, 8, 10 and 12.

level $Y = 5$ above the jet axis. We see that there is an 'overshooting' of the velocity behind the shock, which then gradually relaxes to the steady solutions (1.4) and (1.5) as $t \to \infty$.

In order to see how the solution depends on the mesh used, we repeated the calculations with various grids and computational domains, some of which are listed in table 1. A comparison of the corresponding solutions is presented in figure 5, where the velocity distribution along the jet axis is shown at $t = 5$. One can see that the mesh refinement leads to characteristic steepening of the shock, which is typical for discontinuous solutions.

Another important conclusion that may be drawn from these calculations is that the pseudo-shock always stays perpendicular to the $x$-axis. Indeed, comparing figures 3 and 4, one can see that at each time $t$ the discontinuity happens at the same $x$-position for both $Y = 0$ and $Y = 5$. This result could be anticipated. Indeed, since the

https://doi.org/10.1017/S0022112008003303 Published online by Cambridge University Press

| | $\Delta x$ | $\Delta Y$ | $\Delta t$ | $Y_{\max}$ |
|---|---|---|---|---|
| Mesh 1 | 0.01 | 0.05 | 0.05 | 15 |
| Mesh 2 | 0.02 | 0.1 | 0.1 | 15 |
| Mesh 3 | 0.005 | 0.025 | 0.01 | 15 |
| Mesh 4 | 0.005 | 0.025 | 0.01 | 10 |

TABLE 1. Mesh parameters.

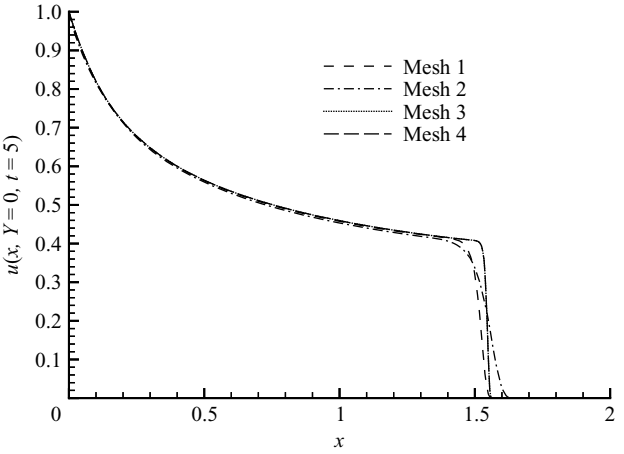



FIGURE 5. Velocity distribution along the jet axis at $t = 5$ for the mesh parameters outlined in table 1.

momentum equation (2.3*a*) contains a term $\partial^2 u/\partial Y^2$, any discontinuity in $Y$-direction has to be smeared out immediately.

## 4. Internal structure of the shock

The pseudo-shocks appear as discontinuities in the velocity field only when observed on the boundary-layer scale, $\hat{x}/L = O(1)$, $\hat{y}/L = O(Re^{-1/2})$. Recall that the boundary-layer approximation does not allow the pressure to change across the jet. However, in order to describe the abrupt change of the fluid velocity in the shock, and the process of the fluid eruption from the jet, one needs to 'restore' the pressure gradient in the governing equations of motion. This may be done by assuming that the pseudo-shock thickness $\Delta x$ is an $O(Re^{-1/2})$ quantity.

It should be noticed that the thickness of classical shock waves in gas dynamics is comparable with the molecular mean free path, which makes the continuum hypothesis inapplicable for describing the internal shock structure. The pseudo-shock we are dealing with in this study is much thicker, and may be investigated using the Navier–Stokes equations.

We denote the position of the shock at time $t$ by $x_s(t)$ and its velocity by $u_s(t) = \dot{x}(t)$. Our task will be to study the flow behaviour in the region where

$$X = \frac{\hat{x}/L - x_s(t)}{Re^{-1/2}}, \qquad Y = \frac{\hat{y}/L}{Re^{-1/2}} \tag{4.1}$$

are order one quantities. We shall call it the inner region.

https://doi.org/10.1017/S0022112008003303 Published online by Cambridge University Press

Being guided by the form of the solution in the jet (§§2 and 3) and by the formalism of the method of matched asymptotic expansions, we represent the fluid dynamic functions in the inner region in the form

$$\hat{u} = U_0\{u_s(t) + U(X, Y, t) + \cdots\}, \qquad \hat{v} = U_0 V(X, Y, t) + \cdots, \\ \hat{p} = P_0 + \rho U_0^2 P(X, Y, t) + \cdots. \tag{4.2}$$

Substituting (4.1) and (4.2) into the Navier–Stokes equations and setting $Re \to \infty$ we arrive at the Euler equations

$$U\frac{\partial U}{\partial X} + V\frac{\partial U}{\partial Y} = -\frac{\partial P}{\partial X}, \tag{4.3a}$$

$$U\frac{\partial V}{\partial X} + V\frac{\partial V}{\partial Y} = -\frac{\partial P}{\partial Y}, \tag{4.3b}$$

$$\frac{\partial U}{\partial X} + \frac{\partial V}{\partial Y} = 0. \tag{4.3c}$$

This means that the flow motion in this region obeys the laws of inviscid steady flow theory. In particular, the Bernoulli equation

$$\tfrac{1}{2}(U^2 + V^2) + P = H(\Psi) \tag{4.4}$$

appears to be applicable. The argument $\Psi$ of the function $H(\Psi)$ on the right-hand side of (4.4) is the stream function defined such that

$$U = \frac{\partial \Psi}{\partial Y}, \qquad V = -\frac{\partial \Psi}{\partial X}. \tag{4.5}$$

Let us now perform the matching of the asymptotic expansions (4.2) in the inner region with the asymptotic expansions (2.1) in the conventional boundary layer which was analysed in §§2 and 3. If we first consider the flow immediately behind the pseudo-shock, then we have to set $x = x_s - 0$ in (2.1) and $X = -\infty$ in (4.1). Applying Prandtl's matching rule to the longitudinal velocity component, we have

$$u(x_s, Y, t) = u_s(t) + U(-\infty, Y, t). \tag{4.6}$$

Similarly, for the flow in front of the pseudo-shock, where the fluid is stagnant in the 'laboratory frame',

$$0 = u_s(t) + U(\infty, Y, t). \tag{4.7}$$

In figure 6, the flow in the inner region is sketched as it is viewed in the moving coordinate frame. Notice that the right-hand side boundary BC represents the region before the shock. In the 'laboratory' coordinate frame for the fluid in this region is stagnant. In the moving frame uniform velocity $U_-$ which, according to (4.7), equals but is opposite to the frame velocity, $u_s(t)$, i.e.

$$U_- = -u_s(t). \tag{4.8}$$

The velocity at the jet axis is denoted by $U_+$. Setting $Y = 0$ in (4.6), we have

$$U_+ = u(x_s, 0, t) - u_s(t). \tag{4.9}$$

We shall now show that

$$U_- = -U_+. \tag{4.10}$$

For this purpose we note that the inner region serves to smooth out the velocity field. This means that if we consider the axis of symmetry of the flow (line DC in figure 6),

https://doi.org/10.1017/S0022112008003303 Published online by Cambridge University Press

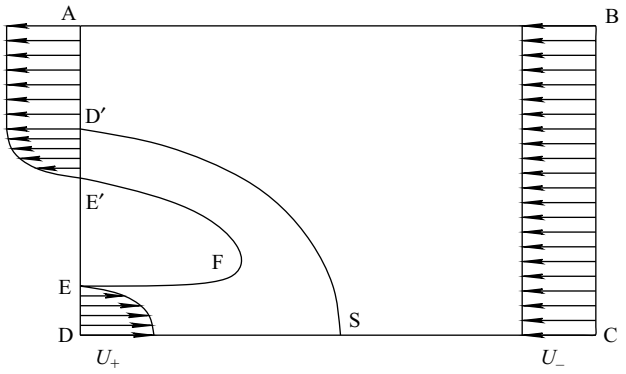



FIGURE 6. Inner structure of the pseudo-shock. Notice that here only the upper half of the flow in the inner region is shown; the lower half is obtained through reflection in the axis of symmetry DC.

then we can expect the velocity to change continuously from a positive value $U_+$ at point D to a negative value $U_-$ at point C. Consequently, between D and C there should exist stagnation point S, where the velocity becomes zero.

Let us apply the Bernoulli equation (4.4) to the two streamlines DS and CS that meet at point S. At point D the pressure is undisturbed, which means that $P$, as defined by (4.2), is zero. As the lateral velocity component $V$ stays zero everywhere on the axis of symmetry DC, applying the Bernoulli equation (4.4) to point D, we can conclude that

$$H = \tfrac{1}{2}U_+^2.$$

Since both velocity components are zeros at point S, we can also write

$$H = P_{\mathrm{S}},$$

where $P_{\mathrm{S}}$ is the value of function $P$ at point S. We see that

$$\tfrac{1}{2}U_+^2 = P_{\mathrm{S}}.$$

Using similar arguments for the streamline CS, we have

$$\tfrac{1}{2}U_-^2 = P_{\mathrm{S}}.$$

This proves that $U_+^2 = U_-^2$. It remains to be taken into account that $U_+$ and $U_-$ have opposite directions, and we can conclude that equation (4.10) holds. Substituting (4.8) and (4.9) into (4.10), we can easily find that the shock velocity is half of the maximum velocity in the jet immediately behind the shock,

$$u_s(t) = \tfrac{1}{2}u(x_s, 0, t).$$

The above formula proves to be in close agreement with laboratory observation of Turner (1962). In his experiments Turner created a jet by supplying salt solution from a roof tank to a downwards pointing orifice. The latter was held just below the surface of a large tank of fresh water. The jet was started suddenly by opening a tap near the orifice. As a result of his measurements, Turner deduced that the jet front propagates with the velocity

$$u_s(t) = 0.49\,u(x_s, 0, t).$$

https://doi.org/10.1017/S0022112008003303 Published online by Cambridge University Press

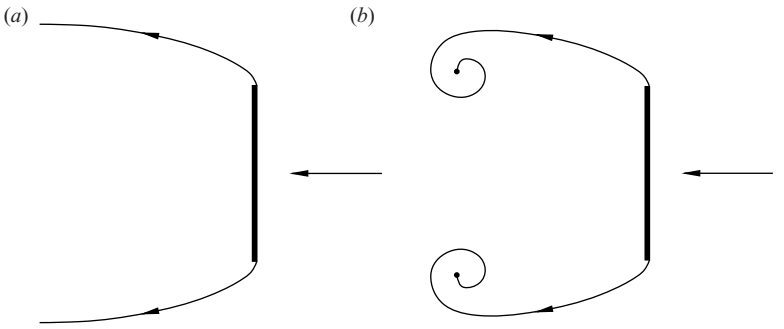



FIGURE 7. Inviscid models of separated flows. (*a*) Kirchoff's (1869) model. (*b*) Tulin's (1964) model.

A more detailed description of the flow in the inner region requires the Euler equations (4.3) to be solved. In order to formulate the boundary conditions for these equations we shall exploit the fact that there is an apparent similarity between the flow considered here and separated flows past rigid bodies. In the inviscid approximation, the study of separated flows has led to the development of the free-streamline theory. A number of flow models have been suggested in the framework of this theory. The first of these was put forward by Kirchhoff as early as 1869. This model is sketched in figure 7(*a*), where, as an example, the flow past a flat plate is shown. Kirchhoff conjectured that as the flow separates at the plate edges, two free streamlines are formed. They separate the main flow from the stagnation region at the rear of the plate. The fluid in the stagnation region is assumed motionless, which makes the pressure constant along the two free streamlines. Kirchhoff (1869) further assumed that the pressure in the stagnation region behind the body equals the unperturbed pressure far upstream of the body. Under this assumption the free streamlines extend to infinity, as shown in figure 6, where due to the flow symmetry, only one of these streamlines, SD′ is shown.

Of course, in the flow depicted in figure 6 we do not have a rigid body. Its role is played by the jet which enters the 'flow domain' through the section DE on the left-hand side boundary, and after collision with the uniform flow BC, leaves the domain through the section E′D′. To accommodate this new circumstance the Kirchhoff theory has to be reformulated accordingly.

We start with elimination of the pressure $P$ from the Euler equations (4.3). This is done through cross-differentiation of equations (4.3*a*) and (4.3*b*). As a result we find that the vorticity

$$\Omega = \frac{\partial V}{\partial X} - \frac{\partial U}{\partial Y} \tag{4.11}$$

does not change along the streamlines. This statement is expressed by the equation

$$U\frac{\partial \Omega}{\partial X} + V\frac{\partial \Omega}{\partial Y} = 0. \tag{4.12}$$

In order to solve (4.12), the vorticity $\Omega$ has to be specified on all the streamlines 'entering' the computational domain (see figure 6). In particular, we know that the flow is uniform at the right-hand-side boundary BC, and therefore, $\Omega = 0$ there. According to (4.12), $\Omega$ will remain zero in the entire region above the streamline SD′ which separates the jet from the rest of the flow. In figure 6 we show that the jet enters the computational domain through section DE of the left-hand-side boundary

https://doi.org/10.1017/S0022112008003303 Published online by Cambridge University Press

AD. It is forced to turn back after 'collision' with the uniform flow BC, and it leaves the domain through section E′D′.

The position of point D′, at which the dividing streamline SD′ crosses the left-hand-side boundary of the computational domain, may be found using the following result of the potential flow theory. Let a semi-infinite body be placed into a uniform flow with velocity $V_\infty$ directed parallel but opposite to the $\hat{x}$-axis. Further let the body be symmetric with respect to the $\hat{x}$-axis, and its contour be such that

$$\hat{y} = a(-\hat{x})^\alpha + \cdots \quad \text{as} \quad \hat{x} \to -\infty. \tag{4.13}$$

Then, independent of the body shape near its nose, the drag of the body

$$D = 2\int_0^\infty (\hat{p} - p_\infty)\,\mathrm{d}\hat{y}$$

may be calculated as

$$D = \begin{cases} 0 & \text{if } \alpha < \frac{1}{2}, \\ \frac{1}{4}\rho V_\infty^2 a^2 \pi & \text{if } \alpha = \frac{1}{2}, \\ \infty & \text{if } \alpha > \frac{1}{2}. \end{cases} \tag{4.14}$$

Here $p_\infty$ is the pressure in the oncoming flow, and $\rho$ the fluid density. All the variables used in (4.13) and (4.14) are dimensional.

The flow in the inner region (see figure 6) is inviscid, and therefore, any streamline can be 'frozen', i.e. treated as the body surface. Obviously, the separating streamline SD′ forms a semi-infinite body, and formula (4.14) may be used to calculate the force $D$ experienced by this body.

Alternatively, $D$ may be calculated through making use of the integral momentum equation. We shall apply it to the control volume DSD′ occupied by the jet (see figure 6). Notice that the jet enters the control volume through the section DE and leaves it through the section E′D′. Keeping in mind that in the stagnation region EFE′ the pressure stays constant, one can use the Bernoulli equation (4.4) to draw the following conclusion. The velocity of a fluid particle as it leaves the control volume through E′D′ is equal to the velocity of this fluid particle as it enters the control volume through DE. This means that the velocity profile across E′D′ is simply a mirror reflection of the velocity profile across DE. Consequently, the integral momentum equation gives

$$D = 4\rho \int_0^{y_0} \hat{u}_{\mathrm{jet}}^2\,\mathrm{d}\hat{y}. \tag{4.15}$$

Here the integration is performed along the section DE; function $\hat{u}_{\mathrm{jet}}(\hat{y})$ represents the velocity profile in the jet, expressed in dimensional variables. It is obtained by solving the boundary-layer equations (2.3), as was done in § 3, and applying the Galileo transformation (4.6). The upper limit $y_0$ of the integration in (4.15) denotes the $\hat{y}$-coordinate of the jet edge E. At this point the Galileo-transformed velocity in the jet becomes zero.

We shall now introduce the non-dimensional variables,

$$\hat{y} = y_0 Y, \qquad \hat{u}_{\mathrm{jet}} = V_\infty U_{\mathrm{jet}}. \tag{4.16}$$

Recall that $V_\infty$ coincides with the pseudo-shock speed, which in its turn is half of the maximum velocity in the jet measured in the laboratory coordinate frame. It should be noticed that $Y$ and $U$ as defined by (4.16) are slightly different from those defined by (4.1) and (4.2). This difference, however, is not important because of the fact that

https://doi.org/10.1017/S0022112008003303 Published online by Cambridge University Press

the Euler equations (4.3) are invariant with respect to the affine transformations

$$X \to AX, \quad Y \to AY, \quad U \to BU, \quad V \to BV, \quad P \to B^2P,$$

where $A$ and $B$ are arbitrary constants.

Substitution of (4.16) into (4.15) leads to

$$D = 4\rho V_\infty^2 y_0 \int_0^1 U_{\text{jet}}^2 \, \mathrm{d}Y. \tag{4.17}$$

Since this quantity is finite, we can conclude that $\alpha$ in (4.13) has to be $1/2$. Then the asymptotic behaviour of the separating streamline appears to be

$$\hat{y} = a(-\hat{x})^{1/2} + \cdots \quad \text{as} \quad \hat{x} \to -\infty, \tag{4.18}$$

and (4.14) is written as

$$D = \tfrac{1}{4}\rho V_\infty^2 a^2 \pi. \tag{4.19}$$

Excluding $a$ from (4.18) and (4.19), we find

$$\hat{y} = 2\sqrt{\frac{D}{\rho V_\infty^2 \pi}}\,(-\hat{x})^{1/2} + \cdots \quad \text{as} \quad \hat{x} \to -\infty. \tag{4.20}$$

It remains to make use of equation (4.17) which, when substituted into (4.20), puts the equation for the separating streamline SD′ into the non-dimensional form

$$Y = 2\kappa(-X)^{1/2} + \cdots \quad \text{as} \quad X \to -\infty. \tag{4.21}$$

Here, $X = \hat{x}/y_0$, $Y = \hat{y}/y_0$ and

$$\kappa = 2\sqrt{\frac{1}{\pi}\int_0^1 U_{\text{jet}}^2 dY}.$$

Equation (4.21) is used to determine the position of point D′ where the separating streamline SD′ crosses the boundary of computational domain ABCD (see figure 6). In order to determine the velocity distribution along D′A, AB and BC, we note that the flow above the separating streamline SD′ is potential ($\Omega = 0$). Consequently, we can introduce the complex conjugate velocity $\overline{V} = U - \mathrm{i}V$. Corresponding to (4.21), the far field behaviour of $\overline{V}$ is given by

$$\overline{V} = -1 + \kappa Z^{-1/2} + \cdots \quad \text{as} \quad Z = X + \mathrm{i}Y \to \infty. \tag{4.22}$$

This solution is obtained by seeking a function $\overline{V}(Z)$ such that it (i) is analytic in the potential part of the flow, (ii) satisfies the symmetry condition $V = 0$ on the axis of symmetry of the flow (SC in figure 6) and (iii) satisfies the impermeability condition on the separating streamline SD′. The first of these conditions is obviously satisfied by function (4.22). In order to verify the second condition we assume that $Z$ is real and positive. Then $\overline{V}$ as given by (4.22) proves to be real, which means that $V = -\mathrm{Im}\overline{V}$ is zero, as required. Finally, on the separating streamline SD′ at large distance from the stagnation point S we can write $Z = (-X)\mathrm{e}^{\mathrm{i}\pi}$ which, being substituted into (4.22), yields

$$U = -1, \qquad V = \kappa(-X)^{-1/2}.$$

The shape of the separating streamline may be now determined from the equation

$$\frac{\mathrm{d}Y}{\mathrm{d}X} = \frac{V}{U} = -\kappa(-X)^{-1/2}. \tag{4.23}$$

One can easily verify that integration of (4.23) recovers the asymptotic formula (4.21).

https://doi.org/10.1017/S0022112008003303 Published online by Cambridge University Press

Let us now consider the complex potential $W = \Phi + \mathrm{i}\Psi$, where $\Phi$ is the velocity potential and $\Psi$ stream function. It is known that

$$\frac{\mathrm{d}W}{\mathrm{d}Z} = \overline{V}. \tag{4.24}$$

Substituting (4.22) into (4.24) and performing the integration, we find

$$W = -Z + 2\kappa Z^{1/2} + \cdots \quad \text{as} \quad Z \to \infty. \tag{4.25}$$

In order to determine the asymptotic behaviour of the stream function $\Psi$, one needs to separate the imaginary part of (4.25). We have

$$\Psi = -Y + 2\kappa \sqrt{\tfrac{1}{2}\sqrt{X^2 + Y^2} - \tfrac{1}{2}X} + \cdots \quad \text{as} \quad X^2 + Y^2 \to \infty. \tag{4.26}$$

### 4.1. *Numerical results*

Substitution of (4.5) into (4.11) leads to the Helmholtz equation

$$\frac{\partial^2 \Psi}{\partial X^2} + \frac{\partial^2 \Psi}{\partial Y^2} = -\Omega. \tag{4.27}$$

The vorticity $\Omega$ on the right-hand side of (4.27) has to be found using equation (4.12). For computational purposes we shall modify it to the form

$$U\frac{\partial \Omega}{\partial X} + V\frac{\partial \Omega}{\partial Y} = \varepsilon\left(\frac{\partial^2 \Omega}{\partial X^2} + \frac{\partial^2 \Omega}{\partial Y^2}\right). \tag{4.28}$$

The reason for this is that the flow considered is susceptible to the Kelvin–Helmholtz instability developing in the returning jet (E′D′ in figure 6). Our calculations show that the instability may be suppressed with the artificial viscosity $\varepsilon$ as small as 0.01.

The boundary conditions for (4.27) and (4.28) were set up in the following way. The asymptotic formula (4.26) was used to determine the stream function distribution along the right-hand-side boundary BC of the computational domain, along the top boundary AB and on the section AD′ of the left-hand-side boundary. The position of point D′, where the separating streamline crosses the left-hand-side boundary, was found by solving numerically the equation that results from setting (4.26) to zero. The stream function distribution on the section DD′ depends on the solution of the boundary-layer equations (2.3). As this solution is changing with time $t$, the velocity profile $U_{\mathrm{jet}}(Y)$ in the jet 'entering' into the computational domain through section DE is also changing. Therefore, as an illustration, a representative solution was calculated assuming simply that

$$U_{\mathrm{jet}}(Y) = 1 - Y^2. \tag{4.29}$$

Integration of (4.29) gives the stream function distribution on DE,

$$\Psi = Y - \tfrac{1}{3}Y^3. \tag{4.30}$$

The stream function distribution on E′D′ is a mirror reflection of (4.30). Finally, on the section EE′ the stream function stays constant, $\Psi = \frac{2}{3}$. This condition ensures that the fluid velocity is zero and pressure is constant all over the stagnant fluid region that lies to the left of the outer edge EFE′ of the jet (see figure 6).

Turning now to the boundary conditions for equation (4.28), one can see that the vorticity $\Omega$ is zero along the right-hand-side boundary BC, at the top AB of the computational domain and on the section AD′ of the left-hand-side boundary. The distribution of $\Omega$ on the interval DE is found by differentiating (4.29). On EE′ the vorticity is zero, and on E′D′ it is obtained by mirror reflection of the vorticity distribution on DE.

https://doi.org/10.1017/S0022112008003303 Published online by Cambridge University Press

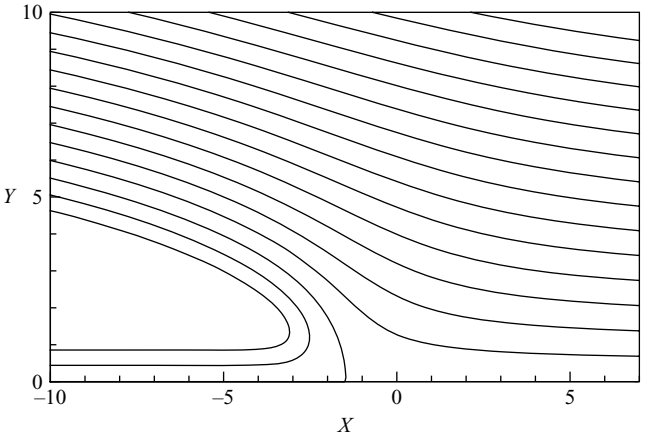



FIGURE 8. The results of the flow calculation in the inner $O(Re^{-1/2}) \times O(Re^{-1/2})$ region. In the jet region the streamlines are plotted corresponding to $\Psi = -0.7$, $-0.45$ and 0. The rest of the streamlines are plotted with the interval $\Delta\Psi = 0.5$.

Equation (4.27) was finite-differenced by using central differences for both terms on the left-hand side. For the two terms on the left-hand side of equation (4.28) the second-order windward differences were used, while the derivatives on the right-hand side of (4.28) were represented by central differences. Both point and line relaxations were tried to solve the problem. The artificial viscosity had to be taken $\varepsilon = 0.01$ or larger to produce a converged solution. Still, the line relaxation required rather deep under-relaxation for the iteration process to converge. As a result it did not bring expected savings in the computational time.

We found that as many as $400 \times 200$ points are required for the solution to be mesh independent. We also found that the computational region should be as big as $X \in [-50, 50]$, $Y \in [0, 50]$. The results of the calculations are shown in figure 8 in the form of the streamline pattern. One has to remember, of course, that the flow is symmetrical with respect to the jet axis and, therefore, only the upper half of the flow field is displayed in figure 8. We see that the solution possesses all the desired properties, which confirms the validity of the suggested flow model.

## 5. Discussion

The main objective of this study is to demonstrate that the classical boundary-layer equations admit discontinuous solutions. For this purpose we consider, as an example, the problem of a laminar jet which emerges from a narrow slit in a wall and penetrates into otherwise stagnant fluid. The steady jet of this kind was analysed by Schlichting in 1933. He found that, provided the slit width is small enough, the steady boundary-layer equations allow for a self-similar solution in the form (1.4) with function $f(\eta)$ satisfying an ordinary differential equation, whose solution (1.5) proved to be surprisingly simple.

In this paper our concern is with the unsteady analogue of Schlichting's problem. We assume that the slit is kept closed until some time, and then when it opens the jet starts to penetrate into the stagnant fluid. To study this process we first produce

https://doi.org/10.1017/S0022112008003303 Published online by Cambridge University Press

the corresponding numerical solution of unsteady boundary-layer equations. The solution shows that the jet has a well-established front representing a discontinuity in the velocity field, similar to the shock waves that form in supersonic gas flows.

Then, in order to reveal the 'internal structure' of the shock we turn to the analysis of the flow in a small region surrounding the discontinuity. With $Re$ denoting the Reynolds number, the size of the inner region is estimated as an order $Re^{-1/2}$ quantity in both longitudinal and lateral directions. We found that the fluid motion in this region is predominantly inviscid and may be treated as quasi-steady if considered in the coordinate frame moving with the jet front. These simplifications allow us to deduce a simple formula for the front speed, which proved to be in close agreement with experimental observation of Turner (1962). Also a detailed description of the flow in the inner region is produced through numerical solution of the Euler equations (4.3) that govern the fluid motion in this region. The 'far field' boundary conditions for these equations are formulated based on the Kirchhoff (1869) model of the free streamline theory.

When using the method of matched asymptotic expansions, as we have done in this study, one has, firstly, to choose the dimensions of the inner and outer region. Secondly, the form of the asymptotic expansions should be chosen correctly for both regions. These choices are then validated by ensuring that the resulting asymptotic equations in the two regions yield solutions that may be properly matched with one another. Since these requirements are fully met in the above analysis, we can claim that the flow model suggested in this study is mathematically self-consistent.

As far as the physical content of the theory is concerned, there is still room for refinement. Most notably, the returning jet (D′E′ in figure 6) has the velocity profile typical of shear layers, and therefore, is susceptible to the Kelvin–Helmholtz instability. This form of instability is known to lead to a roll up of a shear layer (see Nikolskii 1957*a*, *b*; Sudakov 1974; Zakharov 1976, among others). Similar behaviour has to be expected of the returning jet, and, indeed, experimental observations show (see, for example, Pera & Gebhart 1975) that the returning jet can roll into a spiral vortex. In order to incorporate this effect into the theory, one can make use of the Tulin (1964) model (see figure 7*b*). However, adjustment of this model for our problem proves to be a significantly more complicated task than that for the Kirchhoff model (figure 7*a*). We shall leave it for a future publication, and conclude this discussion with the following important comment.

Importantly, the choice of the flow model for the inner region has no effect on the boundary-layer behaviour in the outer region. Indeed, with the Kirchhoff model the pressure in region EFE′ (figure 6) returns to its unperturbed value, which means that the pressure at the outer edge of the boundary layer stays unperturbed, and equations (2.2) can, indeed, be reduced to (2.3). If, instead, we consider the Tulin model (see figure 6*b*), then keeping in mind that the velocity in the inner region remains an order-one quantity, the circulation around the spiral vortex may be estimated as $\Gamma \sim Re^{-1/2}$. This means that in the outer region the pressure perturbations produced by the vortex can be disregarded in the leading-order approximations, and (2.3) still remains valid.

Finally, if one wants to use this theory for practical applications, especially when the large time behaviour of the jet is of interest, then the classical boundary layer model (1.1)–(1.3) might need to be modified as suggested by Schneider (1985). Analysing steady jets, he noticed that the momentum flux (1.6) starts to change as the distance $x$ from the jet origin becomes large. This effect is especially noticeable for axisymmetric jets.

https://doi.org/10.1017/S0022112008003303 Published online by Cambridge University Press

## REFERENCES


Allen, T. & Riley, N. 1994 The three-dimensional boundary layer on a yawed body of revolution. *J. Engng Maths* **28**(5), 345–364.

Degani, A. T., Li, Q. & Walker, J. D. A. 1996 Unsteady separation from the leading edge of an airfoil. *Phys. Fluids* **8**(3), 181–206.

Goldstein, S. 1948 On laminar boundary-layer flow near a position of separation. *Q. J. Mech. Appl. Maths* **1**(1), 43–69.

Kirchhoff, G. 1869 Zur theorie freier flüssigkeitsstrahlen. *J. Reine Angew. Math.* **70**(4), 289–298.

Kluwick, A. & Wohlfahrt, H. 1986 Hot-wire-anemometer study of the entry flow in a curved duct. *J. Fluid Mech.* **165**, 335–353.

Messiter, A. F. 1970 Boundary-layer flow near the trailing edge of a flat plate. *SIAM J. Appl. Maths* **18**(1), 241–257.

Neiland, V. Ya. 1969 Theory of laminar boundary layer separation in supersonic flow. *Izv. Akad. Nauk SSSR, Mech. Zhidk. Gaza* (4), 53–57.

Nikolskii, A. A. 1957*a* The force produced by the 'second form' of fluid motion on two-dimensional bodies (dynamics of two-dimensional separated flows). *Dokl. Akad. Nauk SSSR* **116**(3), 365–368.

Nikolskii, A. A. 1957*b* On the 'second form' of the motion of an ideal fluid around a body (a study of separated vortex flows). *Dokl. Akad. Nauk SSSR* **116**(2), 193–196.

Pera, L. & Gebhart, B. 1975 Laminar plume interactions. *J. Fluid Mech.* **68**, 259–271.

Prandtl, L. 1904 Über flüssigkeitsbewegung bei sehr kleiner Reibung. In *Verh. III. Intern. Math. Kongr., Heidelberg*, pp. 484–491. Teubner, Leipzig, 1905.

Schlichting, H. 1933 Laminare strahlausbreitung. *Z. Angew. Math. Mech.* **13**, 260.

Schneider, W. 1985 Decay of momentum flux in submerged jets. *J. Fluid Mech.* **154**, 91–110.

Stewartson, K. 1969 On the flow near the trailing edge of a flat plate. *Mathematika* **16**(1), 106–121.

Stewartson, K., Cebeci, T. & Chang, K. C. 1980 A boundary layer collision in a curved duct. *Q. J. Mech. Appl. Maths* **33**, 59–75.

Stewartson, K. & Williams, P. G. 1969 Self-induced separation. *Proc. R. Soc. Lond.* A **312**, 181–206.

Sudakov, G. G. 1974 Calculation of the separated flow past a small aspect ratio delta wing. *Uch. Zap. TsAGI* **5**(2), 10–18.

Sychev, V. V. 1972 Laminar separation. *Izv. Akad. Nauk SSSR, Mech. Zhidk. Gaza* (3), 47–59.

Sychev, V. V., Ruban, A. I., Sychev, Vic. V. & Korolev, G. L. 1998 *Asymptotic Theory of Separated Flows*. Cambridge University Press.

Tulin, M. P. 1964 Supercavitating flows – Small perturbation theory. *J. Ship Res.* **7**(3), 16–37.

Turner, J. S. 1962 The 'starting plume' in neutral surroundings. *J. Fluid Mech.* **13**, 356–368.

Zakharov, S. B. 1976 Calculation of inviscid separated flow past a thin circular cone at large angle of attack. *Uch. Zap. TsAGI* **7**(6), 111–116.


https://doi.org/10.1017/S0022112008003303 Published online by Cambridge University Press